Scripta Materialia 107 (2015) 79–82

Contents lists available at ScienceDirect

Scripta Materialia

journal homepage: www.elsevier.com/locate/scriptamat

On the nature of the omega tri-layer periodicity in rapidly cooled Ti-15Mo

J.M. Bennett [a], J.S. Barnard [a], H.J. Stone [a], P.A. Midgley [a], D. Rugg [b], N.G. Jones [a,*]

[a] Department of Materials Science and Metallurgy, University of Cambridge, Cambridge CB3 0FS, UK
[b] Rolls-Royce plc, PO Box 31, Derby DE24 8BJ, UK

ARTICLE INFO

Article history:
Received 1 April 2015
Revised 20 May 2015
Accepted 22 May 2015
Available online 1 June 2015

Keywords:
Titanium alloys
Phase transformations
Scanning/transmission electron microscopy (STEM)
High angle annular dark field (HAADF)
Electron energy loss spectroscopy (EELS)

ABSTRACT

High angle annular dark field (HAADF) images of the omega phase in metastable beta titanium alloys exhibit tri-layered periodicity. However, it is unclear if this indicates preferential site occupation, or is related to the structural modification of omega formation. Here, the periodicity was studied using a combination of HAADF imaging and electron energy loss spectroscopy. The results show that there is no preferential site occupancy or ordering and that the observed intensity variations are related to the imaging conditions.

Additions of transition metal elements to titanium are known to stabilise the high temperature beta phase, enabling its metastable retention at room temperature following rapid cooling. However, such material is often reported to contain the omega phase, which forms through the collapse of consecutive pairs of $\{1\,1\,1\}_\beta$ [1–3]. This formation mechanism suggests that the parent beta phase has a soft phonon mode with respect to $\{1\,1\,2\}_\beta$ shear [4], and that the omega phase present following rapid cooling should be compositionally indistinct from the parent matrix at the point of quenching. However, there is evidence to suggest that a chemical alteration accompanies the structural modification [5,6]. Thus, determining the mechanism of omega formation remains an intriguing question.

The nature of the omega transformation has been studied extensively through lattice imaging using a transmission electron microscope (TEM) [7–12]. However, phase contrast effects prevented early studies from directly imaging the $\{1\,1\,1\}_\beta$ collapse and compositional information was unobtainable due to the dominance of elastically scattered electrons [13]. Improved atomic column resolution and contrast have been achieved by sampling only the incoherently scattered electrons using a high angle annular detector in a scanning-TEM (STEM) [5,13,14]. Recently, interest in the omega phase and its effect on subsequent phase transformations [15–21] have led to new observations through high angle annular dark field (HAADF) imaging [13,22–24].

In HAADF images of Ti–5Al–5Mo–5V–3Cr (wt.%), intensity variations have been observed, with the collapsing planes exhibiting a lower intensity than the non-collapsing planes [24]. This intensity difference has been attributed to variations in the average atomic number of each column of atoms, suggesting preferential site occupation and, possibly, ordering within the omega phase. Intensity variations between the collapsing and non-collapsing planes have also been observed in rapidly cooled Ti–18Mo (wt.%) [13]. Similarly, tri-layered structures have been reported in HAADF images of Gum metal (Ti–31.9Nb–2.0Ta–2.7Zr–0.3O wt.%) [22]. However, multi-slice scattering simulations suggest that the observed intensity variations could also be related to the structural modification of the omega phase rather than compositional effects [14,22]. To date, no compositional data directly related to a tri-layer omega HAADF feature have been presented, without which, it is impossible to ascertain the source of the observed intensity variations.

In the present work, the tri-layer periodicity of omega precipitates within Ti–15Mo (wt.%) has been studied using HAADF STEM imaging coupled with electron energy loss spectroscopy (EELS). The data suggest that the intensity variations are not related to preferential site occupation but are a result of the imaging conditions within the microscope.

A 10 mm diameter rolled bar of Ti–15Mo (wt.%) was supplied by Rolls-Royce plc. A section of this bar was encapsulated in a quartz glass ampoule under an argon atmosphere and heat treated for one hour at 785 °C, ~10 °C above the beta transus temperature, followed by water quenching. Electron transparent samples were

* Corresponding author. Tel.: +44 1223 334367.
E-mail address: ngj22@cam.ac.uk (N.G. Jones).

http://dx.doi.org/10.1016/j.scriptamat.2015.05.025
1359-6462/

produced by twin jet electropolishing using a solution of 8% $HClO_4$ in CH_3OH at −35 °C.

Electron lattice imaging was conducted using a FEI Titan^3 STEM with multiple nested annular dark field (ADF) detectors, which enabled the simultaneous acquisition of images at different inner collection angles. The microscope was operated at 300 kV and was aberration corrected to achieve atomic resolution for both low and high angle annular dark field images, LAADF and HAADF respectively. The inner collection angle for LAADF and HAADF imaging were 26.0 and 79.6 mrad respectively. Images were filtered using the average background subtraction (ABS) procedure in digital micrograph [25], which removed the amorphous components and enhanced periodic features [26].

The microscope was also equipped with an EELS system, which was used to map the compositional variations of the material within the area of interest. Electron loss energies between 200 and 700 eV were measured as a function of position, using a 0.5 Å step size and 0.02 s acquisition period at each point. The Ti L_2 (462 eV) and L_3 (456 eV) edges were isolated using a Poisson noise decomposition and a blind source separation in HyperSpy [27,28] to enable the relative level of Ti atoms in the sampled columns to be displayed as a function of position.

Simulated LAADF and HAADF images were produced via a multi-slice approach using stemslic [29]. The microscope conditions were modelled using; 300 kV, an objective aperture of 19.5 mrad and a defocus of 1 nm. For atom clarity, the lenses were treated as ideal with no aberrations. The exit waves were integrated between angles of 20 and 80 mrad to approximate the experimental LAADF condition, and between 80 and 300 mrad for the HAADF condition.

Two material conditions were considered in the simulations; (i) the perfect beta structure, and (ii) a beta + omega condition. In both cases, 52 layers of Ti atoms were used to simulate the material, giving a total foil thickness of 12 nm. Previous multi-slice simulations of a beta + omega sample described the material as pure beta interspersed with blocks of omega, with the effect of incomplete $\{1\,1\,1\}_\beta$ collapse captured through a series of calculations, each using a different transitional description of the omega structure [22]. However, classical descriptions of athermal omega are based around a soft phonon mode, where the displaced atoms become frozen through rapid cooling [30]. Therefore, in the present manuscript, the omega phase was simulated by allowing each collapsing atom to take up any position between the beta and omega structures, as described by a Weibull probability function with a shape parameter of 3 and a scale parameter of 1.

A raw, unfiltered, HAADF image of the as quenched material along $[0\,1\,1]_\beta$ is shown in Figure 1a. The reduced fast Fourier Transform (FFT) of this image is inset in the figure and provides analogous information to a conventional selected area diffraction pattern. In this case, the frequencies corresponding to the beta reflections have been circled, leaving additional signals at 1/3 and 2/3 of $[2\,\bar{1}\,1]_\beta$ and $[2\,1\,\bar{1}]_\beta$. These frequencies correspond to the two variants of the omega phase that reside within any given $\{0\,1\,1\}_\beta$.

Lattice distortions corresponding to one of the omega variants can be seen within the region enclosed by the white box in Figure 1a. For clarity, this region is magnified in Figure 1b. The omega phase can be identified by a distortion of the $\{1\,1\,1\}_\beta$ with respect to the $[2\,0\,0]_\beta$ when compared to a perfect beta structure. An example of this is contained within the box in Figure 1b. The atomic shifts can be seen more clearly in Figure 1c, which is the same region as Figure 1b following the application of an ABS filter to Figure 1a. With the removal of the amorphous background component, a systematic variation in atom column intensity can be observed, similar to the tri-layer periodicity reported previously in more complicated systems [22,24].

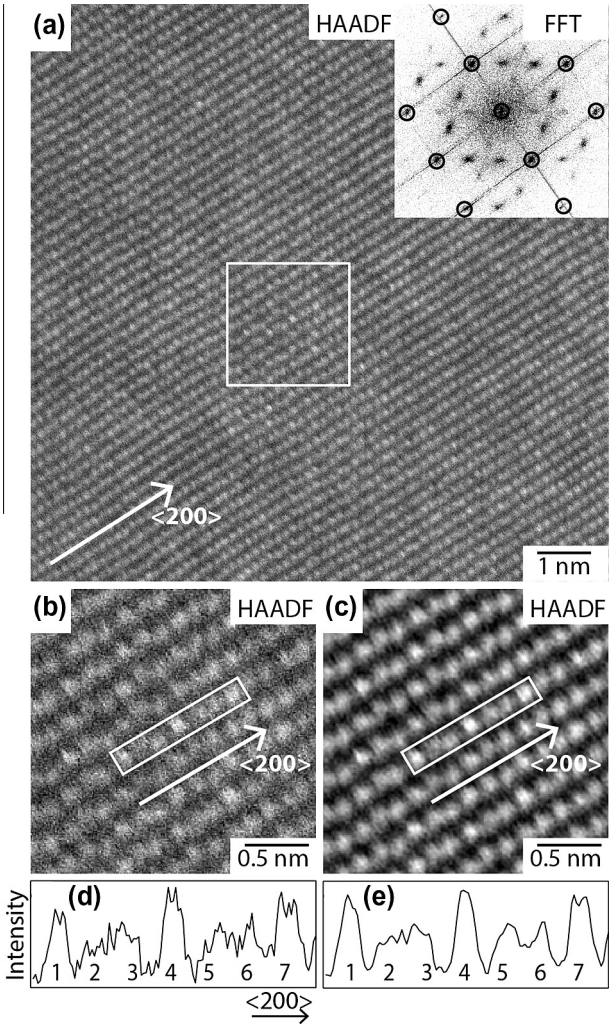

Figure 1. (a) A raw (unfiltered) HAADF image of as quenched Ti–15Mo (wt.%) from a $[0\,1\,1]_\beta$ pole including the corresponding reduced fast Fourier transform (inset); (b) magnified view of the region within the white box shown in part a; (c) ABS filtered counterpart of part b; and (d and e) intensity profiles taken from within the same area as indicated by the boxes in parts b and c.

To visualise this tri-layer periodicity more easily, the intensity within the white boxes in Figure 1b and c, was summed as a function of the position along $[2\,0\,0]_\beta$. The intensity profiles of the boxes are presented in Figure 1d and e for the raw and ABS filtered data respectively. These plots show the summed intensity of seven atom columns, where atom columns 2 and 3 and 5 and 6 contain distortions consistent with the $\{1\,1\,1\}_\beta$ collapse associated with the omega phase. In both the raw and ABS filtered cases, the atom columns in positions 1, 4 and 7 have greater HAADF intensity than those in positions 2, 3, 5 and 6. These observations are entirely consistent with previous studies of Gum metal [22] and Ti–5–5–5–3 [24], which identified the tri-layer periodicity.

HAADF signal is predominantly a result of incoherent scattering and intensity variations are commonly attributed to the atomic number of the species within a given column, $\sim Z^2$. As molybdenum has a higher atomic number than titanium, any preferential site occupation or ordering would be expected to give rise to localised regions of greater intensity. Based on this premise, the results presented in Figure 1 could be interpreted as the molybdenum atoms having a site preference in the omega phase, occupying the non-collapsing planes, i.e. those in positions 1, 4 and 7.

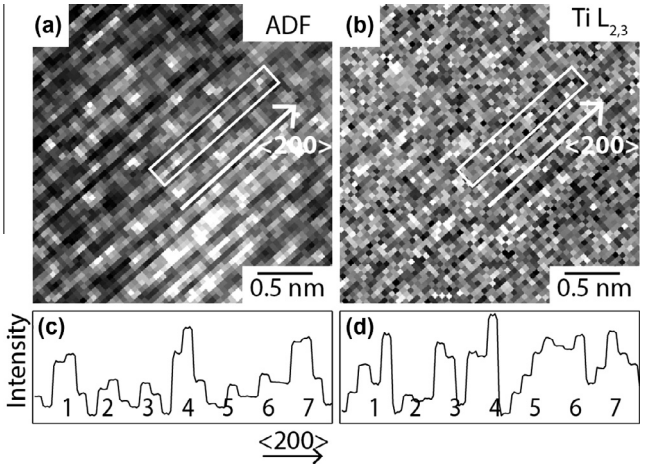

Figure 2. (a) A raw (unfiltered) annular dark field image showing the tri-layer structure; (b) simultaneously acquired Ti EELS map; (c) intensity profile taken from the box marked in part a; and (d) EELS Ti signal taken from the box marked in part b.

To ascertain whether compositional effects are responsible for the tri-layered structure, the same region of material was studied using STEM-EELS. Figure 2a and b show images that were acquired simultaneously from the ADF detector and the Ti $L_{2,3}$ edge component of the EELS spectrum. Despite the imaging resolution being reduced to optimise the EELS signal, the tri-layer periodicity could still be seen in the ADF image and the corresponding box profile shown in Figure 2c. Whilst analysis of the EELS signal from the same box did show variations in Ti signal from each atom column, Figure 2d, these variations did not match the column intensities observed in the ADF image. Therefore, spectroscopy data do not support the idea that the intensity variations observed in Figure 1 are compositionally related.

Recently, Sankaran et al. [22] suggested that the structural alteration associated with the omega transformation could give rise to the observed periodicity and demonstrated this by performing multi-slice HAADF simulations. A similar approach has been followed here, but has been extended to include signal from smaller inner collection angles, and therefore more elastic scattering, in addition to the structural modification.

Multi-slice ADF simulations were performed on two model structures. The first structure represented a perfect beta material, where all atoms were located exactly on their ideal sites. The second structure corresponded to an omega containing beta material, simulated using a frozen phonon approach. Simulated ADF images, corresponding to low (20 mrad, LAADF) and high (80 mrad, HAADF) inner collection angles were calculated for these two structures using only titanium atoms. The resulting images, corresponding to the $[0\,1\,1]_{\beta}$ pole, are shown in Figure 3. When considering a perfect beta structure, Figure 3a and b, no evidence of tri-layer periodicity can be observed. This is unsurprising, as all of the atom positions are well defined and Figure 3b is consistent with that produced in reference [22].

In contrast, the simulated images for the distorted beta structure, Figure 3c and d, show intensity variations between atom columns in the collapsing and non-collapsing planes. Critically, the predicted intensity variation between the two sets of planes is reversed as the inner collection angle changes. This can be seen more clearly in the corresponding box profiles shown in Figure 3e and f. At low collection angles, Figure 3e, the collapsing planes, i.e. numbers 2, 3, 5 and 6, have greater intensities than the non-collapsing planes, 1, 4 and 7. Conversely, at higher collection angles, Figure 3f, the collapsing planes have lower intensities

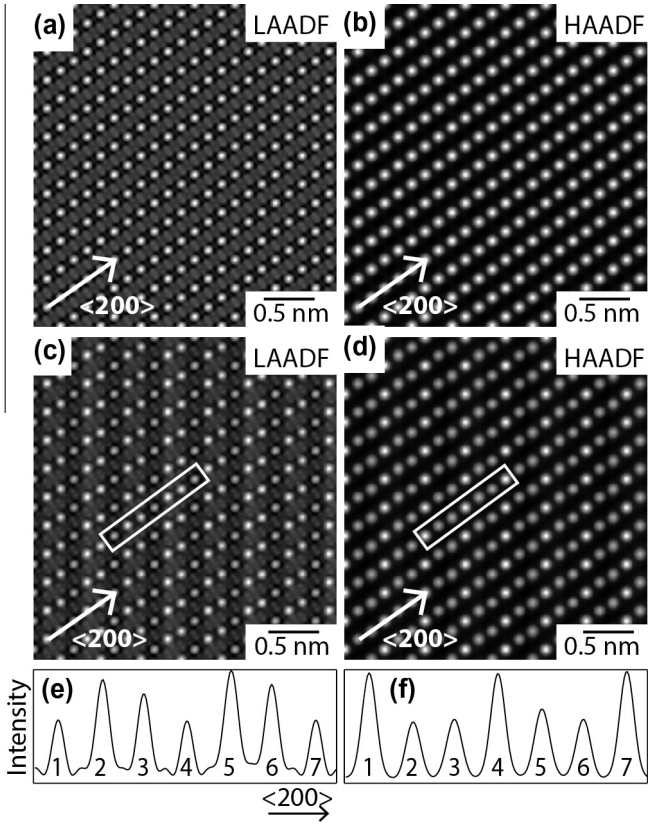

Figure 3. Multi-slice simulations of the perfect beta phase structure in (a) LAADF and (b) HAADF imaging conditions; the modified beta phase structure under (c) LAADF and (d) HAADF imaging conditions; intensity profiles corresponding to (e) the LAADF simulation (white box in part c) and (f) the HAADF simulation (white box in part d).

than the non-collapsing planes. This latter simulation is equivalent to the experimental data presented in Figures 1 and 2, albeit without accounting for any aberrations in the microscope.

The simulated HAADF result for the beta + omega structure is consistent with the work of Sankaran et al. [22]. This similarity is interesting as the previous model incorporated discrete layers of a modified beta structure to represent the omega structure, whereas a frozen phonon approach has been used here. This suggests that any deviation in atom positions, away from the ideal beta structure, can influence the atomic column intensity observed in ADF images. To explore this further, in the present study this analysis was extended to include scattering at smaller inner collection angles.

Using the nested annular detectors in the Titan microscope, it was possible to simultaneously obtain two dark field images at different collection angles, Figure 4. These images were acquired at inner collection angles of 26.0 mrad, Figure 4a, and 79.6 mrad, Figure 4b, from an omega containing region of the sample. The box profiles, Figure 4c and d, show the collapsing planes have a greater intensity than the non-collapsing planes in the LAADF condition, whilst the opposite is true in the HAADF image. These experimental observations are in good agreement with the multi-slice simulations shown in Figure 3, albeit that the magnitude to the intensity variation is less than that predicted. This difference is likely to be related to the number of planes containing perturbations in the sampled atom columns, and within those planes the magnitude of the atomic displacements. Nevertheless, the change in the position of the more intense columns at different collection angles is clearly visible. The consistency between the

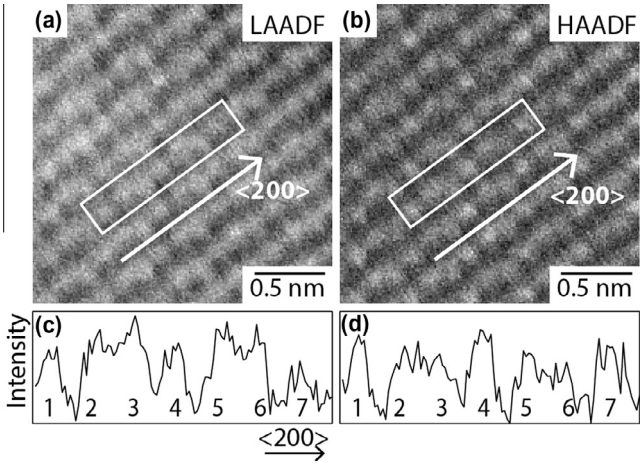

Figure 4. Images of a region containing the omega phase acquired simultaneously under (a) LAADF and (b) HAADF conditions, and (c and d) intensity profiles corresponding to the demarked regions within (a and b).

predicted and observed ADF images under the different microscope conditions and the absence of corresponding compositional variations in the EELS data indicate that the tri-layered structure may be attributed to the imaging conditions rather than compositional effects. The absence of any local preferential site occupation, and the ability of the multi-slice simulations incorporating a frozen phonon approximation of the omega phase to reproduce the experimentally observed features, support the classical description of omega phase formation developed by de Fontaine [4,30].

In this manuscript, the nature of the tri-layered structure associated with the omega phase has been studied using high-resolution ADF imaging and EELS in Ti–15Mo (wt.%). Under HAADF conditions a tri-layer periodicity was observed in material quenched from the beta phase field, which appeared to be associated with the presence of the omega phase. The collapsing planes had lower intensities than those of the non-collapsing planes. Whilst this may be attributed to atomic number contrast and, therefore, that the molybdenum atoms had a site preference within the omega phase, EELS data did not corroborate this interpretation. As a result, the origin of the intensity variation does not appear to be compositionally based. Instead, it is suggested that the tri-layer variation occurs as a result of scattering from atoms displaced from the ideal beta structure as part of the omega phase transformation. Multi-slice ADF simulations indicated that the omega structure could give rise to such periodicity, but that at smaller inner collection angles the variation in intensity between collapsing and non-collapsing planes should change. Simultaneous collection of ADF images at low and high angles confirmed this change, leading to the conclusion that the tri-layered intensity variations observed in HAADF images of Ti-15Mo (wt.%) are structurally driven, and an artefact of the microscope conditions, rather than being related to a compositional site preference.

This work was supported by the Rolls-Royce/EPSRC Strategic Partnership (EP/H022309/1, EP/H500375/1 & EP/M005607/1). The underlying data from this work can be found at the University of Cambridge data repository: https://www.repository.cam.ac.uk/handle/1810/248268.

References

[1] S.K. Sikka, Y.K. Vohra, R. Chidambaram, Prog. Mater. Sci. 27 (1982) 245.
[2] B.S. Hickman, J. Mater. Sci. 4 (1969) 554.
[3] D. de Fontaine, N.E. Paton, J.C. Williams, Acta Metall. 19 (1971) 1153.
[4] D. de Fontaine, Acta Metall. 18 (1970) 275.
[5] S. Nag, A. Devaraj, R. Srinivasan, R. Williams, N. Gupta, G.B. Viswanathan, J.S. Tiley, S. Banerjee, S.G. Srinivasan, H.L. Fraser, Phys. Rev. Lett. 106 (2011) 245701.
[6] J.C. Williams, D. de Fontaine, N.E. Paton, Metall. Trans. 4 (1973) 2701.
[7] M. Hida, E. Sukedai, H. Terauchi, Acta Metall. 36 (1988) 1429.
[8] E. Sukedai, H. Hashimoto, M. Tomita, Philos. Mag. A 64 (1991) 1201.
[9] E. Sukedai, W.Y. Lim, M. Hida, J. Mater. Sci. 28 (1993) 4918.
[10] E. Sukedai, H. Liu, M. Awaji, T. Horiuchi, Ultramicroscopy 54 (1994) 192.
[11] E. Sukedai, Y. Kitano, A. Ohnishi, Micron 28 (1997) 269.
[12] D. Schryvers, L.E. Tanner, Mater. Sci. Forum 56 (1991) 329.
[13] A. Devaraj, S. Nag, R. Srinivasan, R.E.A. Williams, S. Banerjee, R. Banerjee, H.L. Fraser, Acta Mater. 60 (2012) 596.
[14] S.J. Pennycook, D.E. Jesson, Ultramicroscopy 37 (1991) 14.
[15] N.G. Jones, R.J. Dashwood, M. Jackson, D. Dye, Acta Mater. 57 (2009) 3830.
[16] S. Nag, R. Banerjee, R. Srinivasan, J.Y. Hwang, M. Harper, H.L. Fraser, Acta Mater. 57 (2009) 2136.
[17] R.J. Talling, R.J. Dashwood, M. Jackson, D. Dye, Acta Mater. 57 (2009) 1188.
[18] R. Banerjee, S. Nag, H.L. Fraser, Mater. Sci. Eng. C 25 (2005) 282.
[19] H.P. Ng, E. Douguet, C.J. Bettles, B.C. Muddle, Mater. Sci. A 527 (2010) 7017.
[20] N.G. Jones, R.J. Tailing, T.C. Lindley, D. Dye, 12th World Conference on Titanium (2012) 1169.
[21] V.A. Vorontsov, N.G. Jones, K.M. Rahman, D. Dye, Acta Mater. 88 (2015) 323.
[22] R.P. Sankaran, C. Ophus, B. Ozdol, V.R. Radmilovic, A.M. Minor, J.W. Morris Jr., Philos. Mag. 94 (2014) 2900.
[23] M. Ahmed, T. Li, G. Casillas, J.M. Cairney, D. Wexler, E.V. Pereloma, J. Alloys Compd. 629 (2015) 260.
[24] J.C. Sabol, C.J. Marvel, M. Watanabe, T. Pasang, W.Z. Misiolek, Scr. Mater. 92 (2014) 15.
[25] D. Mitchell, B. Schaffer, Ultramicroscopy 103 (2005) 319.
[26] R. Kilaas, J. Microsc. 190 (1998) 45.
[27] HyperSpy, www. Hyperspy.org (2015).
[28] F. de la Peña, M.H. Berger, J.F. Hochepied, F. Dynys, O. Stephan, M. Walls, Ultramicroscopy 111 (2011) 169.
[29] E.J. Kirkland, R.F. Loane, J. Silcox, Ultramicroscopy 23 (1987) 77.
[30] D. de Fontaine, Metall. Trans. A 19 (1988) 169.